Faraday Discussions

Cite this: *Faraday Discuss.*, 2019, **215**, 313

PAPER

Z-scheme photocatalyst systems employing Rh- and Ir-doped metal oxide materials for water splitting under visible light irradiation†

Akihiko Kudo, *[ab] Shunya Yoshino,[a] Taichi Tsuchiya,[a] Yuhei Udagawa,[a] Yukihiro Takahashi,[a] Masaharu Yamaguchi,[a] Ikue Ogasawara,[a] Hiroe Matsumoto[a] and Akihide Iwase [ab]

Received 27th November 2018, Accepted 24th January 2019
DOI: 10.1039/c8fd00209f

Various types of Z-scheme systems for water splitting under visible light irradiation were successfully developed by employing Rh- and Ir-doped metal oxide powdered materials with relatively narrow energy gaps (EG): $BaTa_2O_6$:Ir,La (EG: 1.9–2.0 eV), $NaTaO_3$:Ir,La (EG: 2.1–2.3 eV), $SrTiO_3$:Ir (EG: 1.6–1.8 eV), $NaNbO_3$:Rh,Ba (EG: 2.5 eV) and TiO_2:Rh,Sb (EG: 2.1 eV), with conventional $SrTiO_3$:Rh (an H_2-evolving photocatalyst) or $BiVO_4$ (an O_2-evolving photocatalyst), and suitable electron mediators. The Z-scheme systems were classified into three groups depending on the combination of H_2- and O_2-evolving photocatalysts and electron mediator. The Z-scheme systems combining $BaTa_2O_6$:Ir,La with $BiVO_4$, and $NaTaO_3$:Ir,La with $BiVO_4$ were active when a $[Co(bpy)_3]^{3+/2+}$ redox couple was used rather than an $Fe^{3+/2+}$ one. The combination of $SrTiO_3$:Ir with $SrTiO_3$:Rh gave an activity when the $[Co(bpy)_3]^{3+/2+}$ and $Fe^{3+/2+}$ redox couple ionic mediators were used. The Z-scheme systems combining $NaNbO_3$:Rh,Ba and TiO_2:Rh,Sb with $SrTiO_3$:Rh showed activities by using the $[Co(bpy)_3]^{3+/2+}$ and $Fe^{3+/2+}$ redox couples and also *via* interparticle electron transfer by just contact with/without reduced graphene oxide (RGO). These suitable combinations can be explained based on the impurity levels of doped Rh^{3+} and Ir^{3+} toward the redox potentials of the ionic mediators for the Z-scheme systems employing ionic mediators, and p-/n-type and onset potentials of the photocurrent in the photoelectrochemical properties of those photocatalyst materials for the Z-scheme systems working *via* interparticle electron transfer.

[a]*Department of Applied Chemistry, Faculty of Science, Tokyo University of Science, 1-3 Kagurazaka, Shinjuku-ku, Tokyo 162-8601, Japan. E-mail: a-kudo@rs.kagu.tus.ac.jp*

[b]*Photocatalysis International Research Center, Research Institute for Science and Technology, Tokyo University of Science, 2641, Yamazaki, Noda-shi, Chiba-ken 278-8510, Japan*

† Electronic supplementary information (ESI) available. See DOI: 10.1039/c8fd00209f

Introduction

Artificial photosynthesis has attracted attention from the view point of solar energy conversion to storable chemical energy. Because solar water splitting is one of the representative reactions, photocatalytic water splitting has extensively been studied.[1–7] Powder-based metal oxide materials are attractive for photocatalytic water splitting because the cost will be low[8–10] and stability will be high compared with other materials such as chalcogenides. Although the efficiency of powder-based photocatalyst systems is behind that of systems of photovoltaic + electrolysis at the present stage, there are some advantages to powder-based photocatalyst systems.

It is crucial to demonstrate a solar water splitting system employing powder-based oxide photocatalysts. The present stage of research of artificial synthesis is along this topic. A reactor system including a gas separation system of evolved hydrogen from oxygen has been studied in addition to the development of photocatalyst materials aimed towards the practical use of solar water splitting.[10] The separation system can be achieved by the use of a suitable separation membrane. Moreover, the safety issue of the co-evolved H_2 and O_2 has also been examined *via* the use of a suitable gas transportation tube. However, even if an excellent reactor system with a gas separation membrane system is established, which photocatalyst is employed for it is still a key issue as high efficient photocatalysts for real solar water splitting into H_2 and O_2 without any sacrificial electron donors and acceptors have not yet been developed. It is essential to develop an efficient photocatalyst for demonstrating a solar water splitting system taking gas separation and safety issues into account.

High efficiency of a photocatalyst can be brought about by a high quantum yield and a response to light with a long wavelength. From this viewpoint, it is vital to develop photocatalysts that can utilize up to 600–700 nm of the solar spectrum. Although the use of noble metals might prevent the photocatalyst materials from practical use, the usage would be allowed if the amount is small and the materials can be recycled.

There are single particulate and Z-scheme systems in powder-based photocatalysts.[2,11] Z-scheme photocatalyst systems have the advantage that photocatalysts active for either H_2 or O_2 evolution can be employed. This means that a Z-scheme system can be constructed with various combinations of H_2- and O_2-evolving photocatalysts.[12–15] $SrTiO_3$:Rh (an H_2-evolving photocatalyst) and $BiVO_4$ (an O_2-evolving photocatalyst) are representative metal oxide materials for the Z-scheme system.[1,2,16] It should be stressed that photocatalyst sheets prepared by a particle transfer method using $SrTiO_3$:Rh,La and $BiVO_4$:Mo powders demonstrate a quantum efficiency of 30% at 420 nm and a solar to hydrogen energy conversion efficiency of 1%.[17–19] This result suggests that the Z-scheme system is a promising photocatalyst system for practical solar water splitting. H_2 evolution separated from O_2 evolution is possible in the Z-scheme system if a suitable reactor is designed.[8] However, this photocatalyst sheet consisting of the $SrTiO_3$:Rh,La and $BiVO_4$:Mo powders responds up to 520 nm because the energy gap (EG) of $SrTiO_3$:Rh,La and the band gap (BG) of $BiVO_4$:Mo are 2.3 eV and 2.4 eV, respectively. So, it is a key issue to develop Z-scheme photocatalyst systems consisting of metal oxide photocatalysts with a response at longer wavelengths than 520 nm.

Transition metal doping is one strategy to make wide band gap photocatalysts responsive to visible light.[1,2] Rh and Ir are effective dopants in this strategy. We have reported that $SrTiO_3$:Rh (EG: 2.3 eV),[20] $SrTiO_3$:Rh,Sb (EG: 2.2–2.4 eV),[21] $SrTiO_3$:Ir (EG: 1.6–1.8 eV),[20,22] $BaTa_2O_6$:Ir,La (EG: 1.9–2.0 eV)[23] and $NaTaO_3$:Ir,La (EG: 2.1–2.3 eV)[24] are active for sacrificial H_2 evolution in the presence of electron donors such as methanol, while $SrTiO_3$:Rh,Sb,[21] $SrTiO_3$:Ir[20] and TiO_2:Rh,Sb (EG: 2.1 eV)[25] are active for sacrificial O_2 evolution in the presence of electron acceptors such as Ag^+. In these photocatalyst materials, the visible light responses are due to electronic transition from the impurity levels formed by the dopants to the conduction bands of the host materials. These energy and band gaps are close to, or narrower than, those of $SrTiO_3$:Rh (EG: 2.3 eV)[20] and $BiVO_4$ (BG: 2.4 eV).[26,27] So, it is attractive to utilize these Rh- and Ir-doped metal oxide photocatalysts for the construction of Z-scheme systems.

There are several types of Z-scheme system employing different electron mediators such as $Fe^{3+/2+}$ and $[Co(bpy)_3]^{3+/2+}$ redox couples,[16,28,29] and reduced graphene oxide (RGO)[30–32] as shown in Fig. 1(a) and (b). Moreover, some Z-scheme systems work even without electron mediators, as shown in Fig. 1(c).[33,34] In this case, electron transfer proceeds through an interface contacted between the particles of the H_2- and O_2-evolving photocatalysts. So, it is important to examine the electron mediator in the Z-scheme system.

In the present paper, sacrificial H_2 and O_2 evolutions over Rh- and Ir-doped metal oxide photocatalysts under visible light irradiation were examined first to see the relationship between the photocatalytic properties and their band structures. Then, these H_2- and O_2-evolving photocatalysts were employed for various types of Z-scheme system for water splitting into H_2 and O_2 in stoichiometric amounts under visible light irradiation, without any sacrificial reagents. The photocatalytic performances for the sacrificial H_2 and O_2 evolutions and the Z-schematic water splitting were discussed based on the band structures and

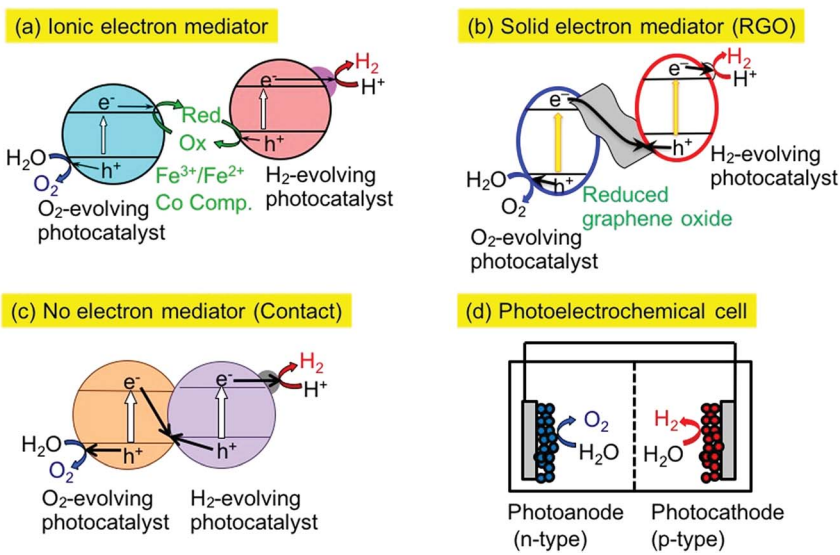

Fig. 1 Various types of powder material-based Z-scheme systems for water splitting.

photoelectrochemical properties of the photocatalyst materials such as p-/n-types and the onset potentials of photocurrents.

Experimental

Preparation of Rh- or Ir-doped metal oxide photocatalysts

$SrTiO_3$:Rh(1%),[29] $SrTiO_3$:Ir(0.2%),[22] TiO_2:Rh(x%),Sb($2x$%) (x = 0.5 or 1.3),[25] $NaTaO_3$:Ir(1%),La(2%),[24] $BaTa_2O_6$:Ir(1%),La(2%)[23] and $BiVO_4$ [26,27] were prepared by a solid-state reaction, a borate-flux method, and a liquid–solid reaction according to previous reports. In addition to them, $NaNbO_3$:Rh(x%),Ba(y%) (x, y) = (1.2, 1.44) or (1.0, 2.0) was newly prepared by a solid-state reaction. The starting materials, Na_2CO_3 (Kanto Chemical; 99.5 or 99.8%), Nb_2O_5 (Kanto Chemical; 99.99% or Kojundo Chemical; 99.99%), Rh_2O_3 (Wako Chemical; 98%), and $BaCO_3$ (Kanto Chemical; 99%), were mixed at a molar ratio of Na/Nb/Rh/Ba = $1.05–1.05y : 1 - x : x : y$. An excess of sodium was added in the starting materials to compensate for volatilization. The starting materials mixture was calcined at 1173 K for 1 h, and then 1423–1473 K for 10 h once or twice. The excess sodium was washed out with water after the calcination. The obtained powders had nonspecific shapes with aggregations, judging from the SEM images (Jeol; JSM-6700F) (Fig. S1†). The obtained samples were identified using X-ray diffraction (Rigaku; MiniFlex, Cu Kα). Diffuse reflectance spectra were obtained by a UV-vis-NIR spectrometer (JASCO, V-570) equipped with an integrator sphere and were converted to absorbance measurements *via* the Kubelka–Munk method.

Preparation of an RGO–metal oxide composite

An RGO-incorporated O_2-evolving photocatalyst was prepared by photocatalytic reduction of graphene oxide (GO) on the photocatalyst according to previous reports.[30–32] GO prepared by the Hummers' method[35] and the O_2-evolving photocatalyst were dispersed in an aqueous methanol (Kanto Chemical; 99.8%) solution (50 vol%). The suspension was irradiated with visible light from a 300 W Xe lamp (PerkinElmer; CERMAX PE300BF) with a long pass filter (HOYA; L42) under a N_2 atmosphere with a pressure of 1 atm to obtain the RGO–photocatalyst composite. The methanol was carefully removed by washing with water. The RGO–photocatalyst composite was collected by filtration and was dried at room temperature in air.

Sacrificial H_2 and O_2 evolutions (half reactions of water splitting)

H_2 and O_2 evolutions from aqueous solutions containing the sacrificial reagents CH_3OH (Kanto Chemical; 99.8%) and $AgNO_3$ (Kojima Chemical; 99.9% or Toyo Chemical; 99.9%) that were half reactions of water splitting were examined using a top-irradiation reaction cell with a Pyrex window and a 300 W Xe lamp (PerkinElmer; CERMAX PE300BF). $NaTaO_3$:Ir,La, $BaTa_2O_6$:Ir,La, $NaNbO_3$:Rh,Ba, and TiO_2:Rh,Sb were used as prepared, whereas $SrTiO_3$:Ir without a cocatalyst was reduced under 1 atm of H_2 at 473 K for 2 h as a pretreatment for sacrificial O_2 evolution. The photocatalyst powders (0.1–0.3 g) were suspended in aqueous solutions (120–150 mL) and irradiated with visible light. For the H_2 evolution, Pt (0.3 wt%) cocatalyst, working as an H_2 evolution site, was loaded on photocatalysts by photodeposition from an aqueous methanol solution containing

H_2PtCl_6 (Tanaka Kikinzoku; 37.55% as Pt). The wavelength of the irradiation light was controlled to visible light using long-pass filters (HOYA; L42 and Y44). The amounts of evolved H_2 and O_2 were determined using an online gas chromatograph (Shimadzu; GC-8A, MS-5A column, TCD, Ar carrier).

Z-schematic water splitting

Z-schematic water splitting was conducted using a gas-closed system with a top-irradiation cell with a Pyrex window. H_2-evolving photocatalyst and O_2-evolving photocatalyst powders (0.05 or 0.1 g, respectively) were suspended in 120 mL of water. For the interparticle Z-scheme systems without an electron mediator and with an RGO solid-state electron mediator, water not containing any ionic mediators was used. For the Z-scheme system with ionic mediator, an aqueous solution containing $[Co(bpy)_3]SO_4$ or $FeCl_3$ as a mediator was used. The pH was adjusted with H_2SO_4 in each of the Z-scheme systems with and without electron mediator, if necessary. Ru (0.7 wt%) cocatalyst, functioning as an H_2 evolution site, was loaded on $SrTiO_3$:Rh (an H_2-evolving photocatalyst) by photodeposition from an aqueous methanol solution containing $RuCl_3 \cdot nH_2O$ (Tanaka Kikinzoku; 36% as Ru in $RuCl_3 \cdot nH_2O$). Pt (0.3–1 wt%) was loaded on the $NaTaO_3$:Ir,La and $BaTa_2O_6$:Ir,La (H_2-evolving photocatalysts), and $SrTiO_3$:Ir (an O_2-evolving photocatalyst) by an impregnation method. The photocatalyst powders and an aqueous H_2PtCl_6 solution were placed in a porcelain crucible and dried on a hot plate. The H_2PtCl_6-impregnated $NaTaO_3$:Ir,La and $BaTa_2O_6$:Ir,La powders were calcined at 673 K for 2 h in air, whereas the $SrTiO_3$:Ir was not. The Pt-loaded $NaTaO_3$:Ir,La and Pt-loaded $BaTa_2O_6$:Ir,La were subsequently reduced at 673 K for 1 h under 1 atm of H_2 as a pretreatment, while Pt-loaded $SrTiO_3$:Ir was reduced at 573 K for 1 h. The light source and GC setup were the same as those for the sacrificial H_2 and O_2 evolutions.

Photoelectrochemical measurements

A squeegee method was used to prepare the $SrTiO_3$:Rh(1%) photoelectrode and a drop-casting method was used for the $NaTaO_3$:Ir(1%),La(2%) and $BaTa_2O_6$:-Ir(1%),La(2%) with and without H_2-reduction; $SrTiO_3$:Ir(0.2%) with H_2-reduction; $NaNbO_3$:Rh(1%),Ba(2%) and TiO_2:Rh(0.5%),Sb(1%) without H_2-reduction, and $BiVO_4$ photoelectrodes using powdered photocatalyst materials. For the $SrTiO_3$:-Rh(1%) photoelectrode, a paste consisting of 20 mg of $SrTiO_3$:Rh(1%) photocatalyst powder, 20 μL of acetylacetone (Kanto Chemical; 99.5%) and 40 μL of distilled water was coated on an indium tin oxide transparent electrode (ITO).[36] For the other photoelectrodes, the photocatalyst powders were dispersed in ethanol (1–2 mg mL^{-1}) by sonication. The suspensions were drop-cast onto a fluorine-doped tin oxide transparent electrode (FTO) to obtain 1–2 mg cm^{-2} of photocatalyst on the FTO. The H_2-reduced $SrTiO_3$:Ir-loaded FTO substrate was not calcined, whereas the other photocatalyst-loaded ITO and FTO substrates were calcined at 573–673 K for 2 h in air. The photoelectrochemical properties were evaluated with a three-electrode system consisting of working, Ag/AgCl reference, and Pt counter electrodes with a potentiostat (Hokuto Denko; HZ-series or HSV-110) using a conventional H-type cell with a Nafion membrane. The electrolyte was 0.1 mol L^{-1} K_2SO_4. 0.025 mol L^{-1} KH_2PO_4 + 0.025 mol L^{-1} Na_2HPO_4 pH buffer

was added, if necessary. A 300 W Xe lamp (PerkinElmer; CERMAX PE300BF) with a long-pass filter (HOYA; L42) was employed as a light source.

Results

Photocatalytic activities for sacrificial H_2 and O_2 evolutions over Rh- and Ir-doped metal oxide materials and their band structures

Sacrificial H_2 and O_2 evolutions of half reactions were carried out as test reactions of water splitting over Rh- and Ir-doped metal oxide photocatalysts using a sacrificial electron donor and acceptor to see the ability for photocatalytic H_2 or O_2 evolution, as shown in Table 1, prior to conducting water splitting.

The energy gaps were determined from the diffuse reflectance spectra and wavelength dependence of the photocatalytic activities as shown in Fig. 2 and 3. In general, trivalent and tetravalent Rh and Ir species are doped at the Ti^{4+}, Nb^{5+} and Ta^{5+} sites in metal oxide materials.[20–25,37,38] Among the species, Rh^{3+} and Ir^{3+} contribute to the visible light response for metal oxide photocatalysts.[20,24,37,38] Sb^{5+} was codoped with Rh^{3+} at the Ti^{4+} and Nb^{5+} sites for charge compensation to enhance the formation of Rh^{3+} and Ir^{3+} and suppress the formation of Rh^{4+} and Ir^{4+} as efficient recombination centers between photogenerated electrons and holes, while Ba^{2+} and La^{3+} were replaced at the alkali and alkaline earth metal sites for the same purpose. $SrTiO_3$:Ir was reduced with H_2 at 473 K to form the dopant Ir^{3+}.

In the case of the Ir-doped photocatalysts, $SrTiO_3$:Ir was active for both the sacrificial H_2 and O_2 evolutions,[20,22] whereas $BaTa_2O_6$:Ir,La and $NaTaO_3$:Ir,La were active only for the sacrificial H_2 evolution.[23,24] $BaTa_2O_6$:Ir,La and $NaTaO_3$:Ir,La were not active for sacrificial O_2 evolution even if they were reduced with H_2 at 673 K, as $SrTiO_3$:Ir was, to reduce the Ir^{4+} species. The Rh-doped photocatalysts

Table 1 Sacrificial H_2 and O_2 evolutions under visible light irradiation over Rh- or Ir-doped metal oxide photocatalysts[a]

Photocatalyst	Energy gap/eV	Incident light/nm	Activity/ μmol h^{-1}		Ref.
			H_2[b]	O_2[c]	
Pt/$NaTaO_3$:Ir(1%),La(2%)	2.1–2.3	$\lambda > 420$	3.2	—	24
$NaTaO_3$:Ir(1%),La(2%)	2.1–2.3	$\lambda > 420$	—	0	24
Pt/$BaTa_2O_6$:Ir(1%),La(2%)	1.9–2.0	$\lambda > 420$	4.6	—	23
$BaTa_2O_6$:Ir(1%),La(2%)	1.9–2.0	$\lambda > 420$	—	0	23
Pt/$SrTiO_3$:Ir(0.2%)	1.6–1.8	$\lambda > 440$	8.6	—	20
$SrTiO_3$:Ir(0.2%)[d]	1.6–1.8	$\lambda > 420$	—	4.3	20
Pt/$NaNbO_3$:Rh(1%),Ba(2%)	2.5	$\lambda > 420$	0.2	—	This work
$NaNbO_3$:Rh(1%),Ba(2%)	2.5	$\lambda > 420$	—	5.3	This work
Pt/TiO_2:Rh(0.5%),Sb(1%)	2.1	$\lambda > 440$	0	—	This work
TiO_2:Rh(0.5%),Sb(1%)	2.1	$\lambda > 440$	—	7.5	25

[a] Photocatalyst: 0.1–0.3 g; light source: 300 W Xe lamp with long-pass filters ($\lambda > 420$ nm or $\lambda > 440$ nm); reaction cell: top-irradiation cell with a Pyrex window. [b] Cocatalyst: Pt (0.3 wt%, photodeposition); reactant solution: 10 vol% aqueous methanol solution. [c] Cocatalyst: none; reactant solution: 0.02–0.05 mol L^{-1} aqueous $AgNO_3$ solution (120–150 mL). [d] Treatment: H_2-reduction at 473 K for 2 h.

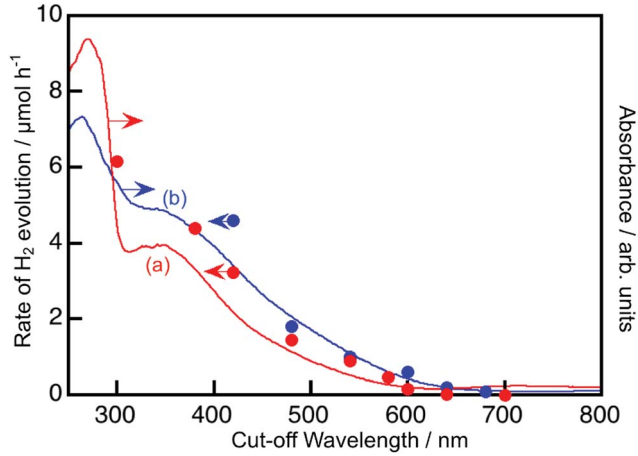

Fig. 2 The wavelength dependence of H_2 evolution from a 10 vol% aqueous methanol solution (closed circles) and diffuse reflectance spectra (solid line) of (a) $NaTaO_3$:Ir(1%),La(2%) and (b) $BaTa_2O_6$:Ir(1%),La(2%). Photocatalyst: 0.1 g, cocatalyst: Pt (photodeposition) for H_2 evolution, reactant solution: 120 mL, light source: 300 W Xe lamp with long-pass filters, and reaction cell: top-irradiation cell with a Pyrex window. Samples of diffuse reflectance spectra were reduced at 473 K.

TiO_2:Rh,Sb[25] and $NaNbO_3$:Rh,Ba were active for sacrificial O_2 evolution using Ag^+ as an electron acceptor. $NaNbO_3$:Rh,Ba showed very low activity for the sacrificial H_2 evolution. These properties will be discussed based on the band structure in the Discussion section. These results of the sacrificial H_2 and O_2 evolutions suggest that $NaTaO_3$:Ir,La and $BaTa_2O_6$:Ir,La can be used as H_2-evolving

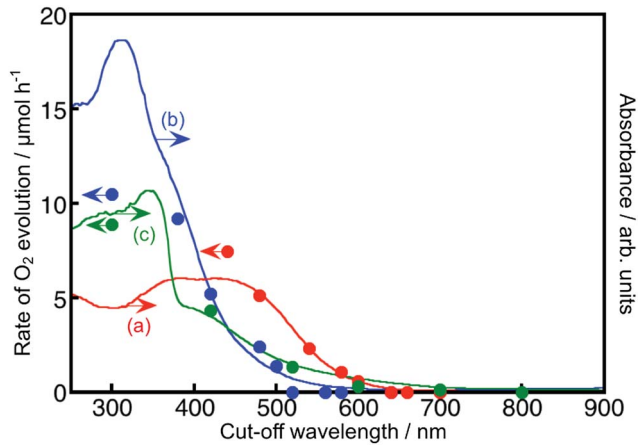

Fig. 3 The wavelength dependence of O_2 evolution from a 0.05 mol L^{-1} aqueous silver nitrate solution (closed circles) and diffuse reflectance spectra (solid line) of (a) TiO_2:Rh(1.3%),Sb(2.6%), (b) $NaNbO_3$:Rh(1.2%),Ba(1.44%) and (c) $SrTiO_3$:Ir(0.2%) with H_2 reduction at 473 K. Photocatalyst: 0.1–0.3 g, reactant solution: 150 mL, light source: 300 W Xe lamp with long-pass filters, and reaction cell: top-irradiation cell with a Pyrex window.

photocatalysts for the construction of Z-scheme systems, while $SrTiO_3$:Ir, $NaNbO_3$:Rh,Ba and TiO_2:Rh,Sb are expected to be employed as O_2-evolving photocatalysts.

Fig. 2 and 3 show the diffuse reflectance spectra and wavelength dependence of the photocatalytic H_2 and O_2 evolutions of the Rh- and Ir-doped metal oxide photocatalysts in the presence of sacrificial reagents. The wavelengths were controlled with long-pass filters. It is vital to see the wavelength dependency of the photocatalytic activity because it is not guaranteed that photocatalysts with visible light absorption bands always give activities under visible light irradiation. The onsets of the wavelength dependence agreed with those of the diffuse reflection spectra. The onset wavelengths for the H_2 evolutions were 640 and 600 nm for $BaTa_2O_6$:Ir,La and $NaTaO_3$:Ir,La, respectively. These onset wavelengths were longer than the 540 nm of $SrTiO_3$:Rh (a conventional H_2-evolving photocatalyst). The onset wavelengths for O_2 evolution were 600, 500 and 700 nm for TiO_2:Rh,Sb, $NaNbO_3$:Rh,Ba and $SrTiO_3$:Ir, respectively. It is noteworthy that TiO_2:Rh,Sb and $SrTiO_3$:Ir responded at longer wavelengths than the $BiVO_4$ (BG: 2.4 eV) (a conventional O_2-evolving photocatalyst).

Fig. 4 shows the band structures of the Rh- and Ir-doped metal oxide photocatalysts. The impurity levels of Rh^{3+} and Ir^{3+} were estimated from the energy gaps determined by diffuse reflection spectra supposing that the valence band consisting of O 2p located at +3 V *vs.* NHE at a pH of 0.[39] The absorption bands in the visible light region shown in Fig. 2 and 3 are due to electronic transition from the impurity levels consisting of Rh^{3+} and Ir^{3+} to the conduction bands of the host materials. The impurity levels formed with electron-filled orbitals of Ir^{3+} were around 1.0–1.2 V for $NaTaO_3$ and $BaTa_2O_6$, while Ir^{3+} in $SrTiO_3$ formed an impurity level around 1.4–1.6 V that was deeper than those in the cases of the tantalates. The energy levels formed with electron-filled orbitals of Rh^{3+} located around 2.0–2.1 V that were similar to those of $SrTiO_3$:Rh and $SrTiO_3$:Rh,Sb.[20,21] The reason Rh^{3+} forms a deeper impurity level than Ir^{3+} is due to Ir^{4+} being more stable than Rh^{4+} in metal oxides. Therefore, electronic transition from the Ir^{3+} impurity level to a conduction band is easier than that from Rh^{3+}, resulting in the formation of the shallow impurity level by Ir^{3+}.

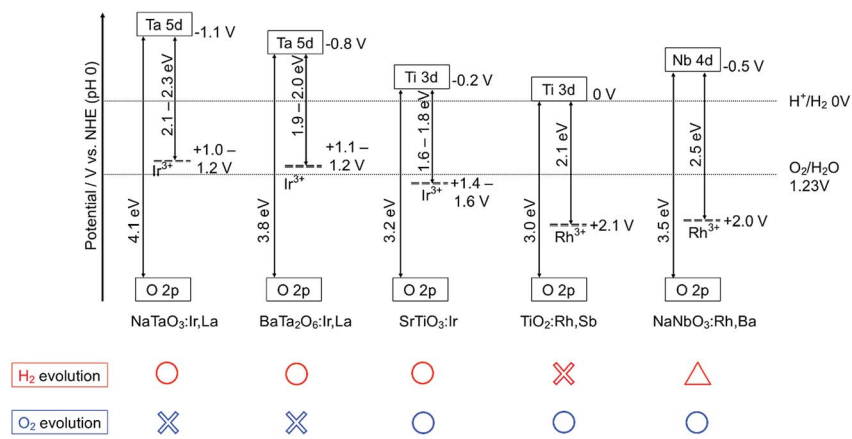

Fig. 4 The band structures of Rh- or Ir-doped metal oxide photocatalysts at pH 0.

Z-schematic systems for photocatalytic water splitting employing Rh- and Ir-doped metal oxide materials

The combination of $SrTiO_3$:Rh and $BiVO_4$ photocatalysts can be a benchmark of a Z-scheme photocatalyst system. The Z-schematic water splitting proceeds using $Fe^{3+/2+}$ and $[Co(bpy)_3]^{3+/2+}$ redox couples as ionic mediators (Fig. 1(a))[16,28,29] and also *via* interparticle electron transfer between $SrTiO_3$:Rh and $BiVO_4$ particles with and without RGO (Fig. 1(b) and (c)).[30,33,34] In general, water splitting *via* Z-schematic interparticle electron transfer by contact between the particles of the H_2- and O_2-evolving photocatalysts with and without RGO can be achieved (Fig. 1(b) and (c)) when the H_2- and O_2-evolving photocatalysts satisfy the following two requirements; (i) H_2- and O_2-evolving photocatalysts possess p- and n-type semiconductor properties, respectively, (ii) there is a certain electrode potential at which the cathodic photocurrent of the p-type semiconductor overlaps with the anodic photocurrent of the n-type semiconductor, being similar to water splitting using a photoelectrochemical cell working with no applied external bias as shown in Fig. 1(d).[31,32] Moreover, H_2- and O_2-evolving photocatalysts must have contact with each other for interparticle electron transfer. In contrast to this, a Z-scheme system employing an ionic electron mediator could work regardless of the p- or n-type properties of the H_2- or O_2-evolving photocatalysts, if the photocatalysts have potentials for the reduction or oxidation of redox couple ionic mediators and the adsorption abilities for the redox couples. The $SrTiO_3$:Rh and $BiVO_4$ photocatalysts satisfy these factors resulting in all of the Z-scheme systems showing activities for water splitting into H_2 and O_2 in stoichiometric amounts without any sacrificial reagents (Fig. 1(a)–(d)).

Various types of Z-scheme photocatalyst systems employing Ir- and Rh-doped photocatalysts for water splitting into H_2 and O_2 under visible light irradiation are shown in Table 2. Here, the absolute evaluation of the performance of photocatalyst systems for water splitting is how much H_2 and O_2 is obtained under certain experimental conditions. In this sense, the activities of the different Z-scheme systems in Table 2 are comparable with each other, but not with those of Table 1, because of the almost identical experimental conditions for the water splitting, even if the kinetics would be different among the systems.

For the construction of Z-scheme systems, $BiVO_4$ (an O_2-evolving photocatalyst) was combined with $BaTa_2O_6$:Ir,La and $NaTaO_3$:Ir,La (H_2-evolving photocatalysts), while $SrTiO_3$:Rh (an H_2-evolving photocatalyst) was combined with TiO_2:Rh,Sb, $NaNbO_3$:Rh,Ba and $SrTiO_3$:Ir (O_2-evolving photocatalysts) as suggested by their H_2 and O_2 evolution abilities. In addition to the suspension system, the photoelectrochemical properties of photocatalyst powders immobilized on a conducting substrate as shown in Fig. 1(d) were examined using a Pt counter electrode without any sacrificial reagents to see the cathodic or anodic photocurrent and the onset potentials of semiconductor properties, not as a water splitting device, as shown in Fig. 5, in order to consider the potential overlap for Z-schematic water splitting *via* interparticle electron transfer with and without RGO. It has been reported that $SrTiO_3$:Rh[36,40] and $BiVO_4$ [32,41–44] function as a photocathode and photoanode, respectively. $NaTaO_3$:Ir,La showed only an anodic photocurrent. Although $BaTa_2O_6$:Ir,La and $SrTiO_3$:Ir showed cathodic and anodic photocurrents, the photocurrents were poor and the onset potentials shifted with the sweeping direction of the CV curves. This result implies that

Table 2 Z-schematic water splitting under visible light irradiation using Rh- or Ir-doped metal oxide photocatalysts[a]

H_2-photocat.	O_2-photocat.	Mediator	Initial pH	Activity/μmol h^{-1}		Ref.
				H_2	O_2	
$Pt/NaTaO_3$:Ir(1%),La(2%)[b]	$BiVO_4$	None[e]	4.2	Trace	Trace	This work
$Pt/NaTaO_3$:Ir(1%),La(2%)[b]	$BiVO_4$	RGO[e]	4.2	Trace	Trace	This work
$Pt/NaTaO_3$:Ir(1%),La(2%)[b]	$BiVO_4$	$Fe^{3+/2+f}$	2.4	Trace	Trace	This work
$Pt/NaTaO_3$:Ir(1%),La(2%)[b]	$BiVO_4$	$[Co(bpy)_3]^{3+/2+g}$	4.2	0.8	0.3	This work
$Pt/BaTa_2O_6$:Ir(1%),La(2%)[b]	$BiVO_4$	None[e]	4.2	0.9	0.4	This work
$Pt/BaTa_2O_6$:Ir(1%),La(2%)[b]	$BiVO_4$	RGO[e]	4.2	0.9	0.4	This work
$Pt/BaTa_2O_6$:Ir(1%),La(2%)[b]	$BiVO_4$	$Fe^{3+/2+f}$	2.4	0.1	0.4	This work
$Pt/BaTa_2O_6$:Ir(1%),La(2%)[b]	$BiVO_4$	$[Co(bpy)_3]^{3+/2+g}$	4.2	5.9	2.1	22
$Ru/SrTiO_3$:Rh(1%)[c]	$Pt/SrTiO_3$:Ir(0.2%)[d]	None[e]	3.5	0.4	Trace	This work
$Ru/SrTiO_3$:Rh(1%)[c]	$Pt/SrTiO_3$:Ir(0.2%)[d]	RGO[e]	3.5	0.8	Trace	This work
$Ru/SrTiO_3$:Rh(1%)[c]	$Pt/SrTiO_3$:Ir(0.2%)[d]	$Fe^{3+/2+f}$	2.4	2.5	1.0	This work
$Ru/SrTiO_3$:Rh(1%)[c]	$Pt/SrTiO_3$:Ir(0.2%)[d]	$[Co(bpy)_3]^{3+/2+h}$	7.8	5.1	2.4	This work
$Ru/SrTiO_3$:Rh(1%)[c]	$NaNbO_3$:Rh(1%),Ba(2%)	None[e]	2.4	2.1	1.1	This work
$Ru/SrTiO_3$:Rh(1%)[c]	$NaNbO_3$:Rh(1%),Ba(2%)	$Fe^{3+/2+f}$	2.4	5.7	2.3	This work
$Ru/SrTiO_3$:Rh(1%)[c]	$NaNbO_3$:Rh(1%),Ba(2%)	$[Co(bpy)_3]^{3+/2+h}$	3.8	4.1	1.7	This work
$Ru/SrTiO_3$:Rh(1%)[c]	TiO_2:Rh(0.5%),Sb(1%)	None[e]	3.5	5.4	2.4	This work
$Ru/SrTiO_3$:Rh(1%)[c]	TiO_2:Rh(0.5%),Sb(1%)	$Fe^{3+/2+f}$	2.4	12	5.3	This work
$Ru/SrTiO_3$:Rh(1%)[c]	TiO_2:Rh(0.5%),Sb(1%)	$[Co(bpy)_3]^{3+/2+h}$	3.5	28	13	This work

[a] Photocatalyst: 0.05 or 0.1 g each; light source: 300 W Xe lamp with a long-pass filter ($\lambda > 420$ nm); reaction cell: top-irradiation cell with a Pyrex window. [b] Cocatalyst: Pt (0.3 wt%, impregnation at 673 K for 2 h and subsequent H_2-reduction at 673 K for 1 h). [c] Cocatalyst: Ru (0.7 wt%, photodeposition). [d] Cocatalyst: Pt (1 wt%, impregnation without calcination and subsequent H_2-reduction at 573 K for 1 h). [e] Reactant solution: H_2SO_4 solution. [f] Reactant solution: 2 mmol L^{-1} $FeCl_3$ solution. [g] Reactant solution: 0.02 mmol L^{-1}. [h] Reactant solution: 0.5 mmol L^{-1} $[Co(bpy)_3]SO_4$ solution (120 mL).

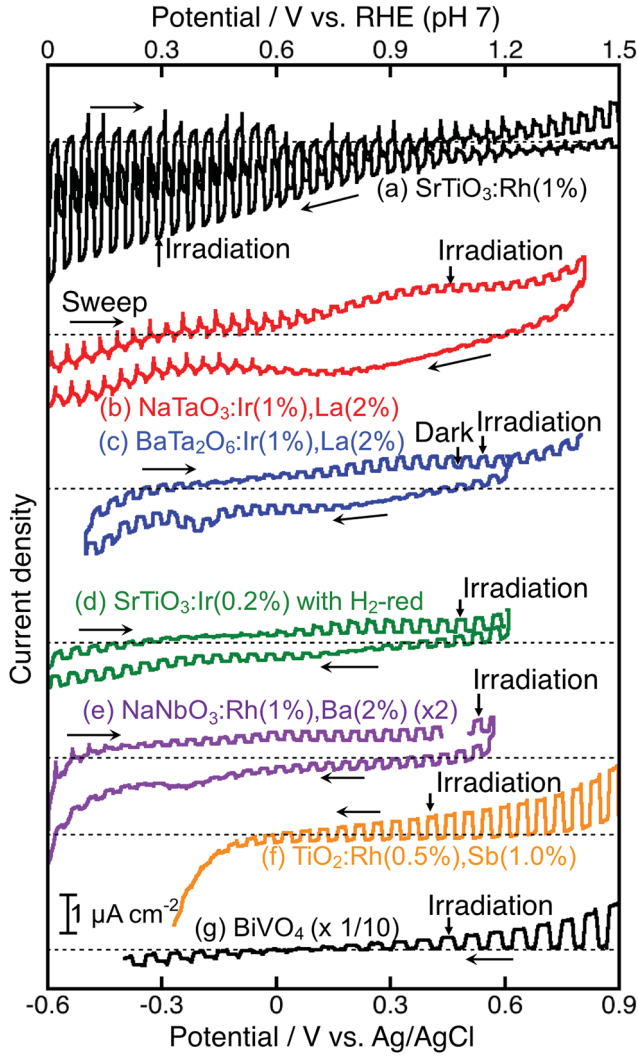

Fig. 5 Current *vs.* potential curves of (a) $SrTiO_3$:Rh(1%), (b) $NaTaO_3$:Ir(1%),La(2%), (c) $BaTa_2O_6$:Ir(1%),La(2%), (d) $SrTiO_3$:Ir(0.2%) with H_2 reduction, (e) $NaNbO_3$:Rh(1%),Ba(2%), (f) TiO_2:Rh(0.5%),Sb(1%), and (g) $BiVO_4$. Electrolyte: 0.1 mol L^{-1} K_2SO_4 aqueous solution (pH 7, phosphate buffer was added if necessary), light source: 300 W Xe lamp ($\lambda > 420$ nm).

those photocurrents might not be due to H_2 and O_2 evolutions, but possibly due to redox reactions of the doped Ir species. In contrast, TiO_2:Rh,Sb,[45] and $NaNbO_3$:Rh,Ba gave clear anodic photocurrents indicating an n-type semiconductor character. The onset potential of $NaNbO_3$:Rh,Ba was more negative than that of TiO_2:Rh,Sb, whereas the anodic photocurrent of $NaNbO_3$:Rh,Ba was much smaller than that of TiO_2:Rh,Sb. These anodic photocurrents overlapped with the cathodic photocurrent of $SrTiO_3$:Rh at a certain electrode potential.

The Z-scheme systems were classified into three groups depending on the combination of H_2- and O_2-evolving photocatalysts and an electron mediator;

being active for only a $[Co(bpy)_3]^{3+/2+}$ redox couple, active for $[Co(bpy)_3]^{3+/2+}$ and $Fe^{3+/2+}$ redox couple ionic mediators, active not only for $[Co(bpy)_3]^{3+/2+}$ and $Fe^{3+/2+}$ redox couples but also *via* interparticle electron transfer with and without RGO. $NaTaO_3$:Ir,La + $BiVO_4$ and $BaTa_2O_6$:Ir,La + $BiVO_4$ were active when not $Fe^{3+/2+}$ but a $[Co(bpy)_3]^{3+/2+}$ redox couple was used. Although the $BaTa_2O_6$:Ir,La + $BiVO_4$ showed activities *via* interparticle electron transfer at a pH of 4.2 with and without RGO, the activities were smaller than that with the ionic electron mediator $[Co(bpy)_3]^{3+/2+}$. $SrTiO_3$:Rh + $SrTiO_3$:Ir was active when the $[Co(bpy)_3]^{3+/2+}$ and $Fe^{3+/2+}$ redox couple ionic mediators were used, whereas it was not active *via* interparticle electron transfer with and without RGO at pH 3.5. $SrTiO_3$:Rh + $NaNbO_3$:Rh,Ba and $SrTiO_3$:Rh + TiO_2:Rh,Sb were active for the $[Co(bpy)_3]^{3+/2+}$ and $Fe^{3+/2+}$ redox couples and *via* interparticle electron transfer without RGO. These Z-scheme systems with RGO using $NaNbO_3$:Rh,Ba and TiO_2:Rh,Sb were not examined in detail, because the GOs were not suitably photoreduced on the $NaNbO_3$:Rh,Ba and TiO_2:Rh,Sb due to their poor reducing activities, as expected from their poor H_2 evolution activities as shown in Table 1. $SrTiO_3$:Rh + TiO_2:Rh,Sb showed the best performances among the Z-scheme systems in Table 2.

Discussion

H_2 and O_2 evolution abilities (shown in Table 1) can be considered based on the band structure, as shown in Fig. 4. Photogenerated holes in the Ir^{3+} levels in $NaTaO_3$:Ir,La and $BaTa_2O_6$:Ir,La have no potentials for water oxidation. In contrast, the Ir^{3+} level of $SrTiO_3$:Ir possesses the water oxidation potential, though the driving force is not so large. Conduction bands consisting of Ta 5d orbitals in $BaTa_2O_6$:Ir,La and $NaTaO_3$:Ir,La possess thermodynamically enough potentials for water reduction to form H_2. On the other hand, the photogenerated holes in the Rh^{3+} levels in $NaNbO_3$:Rh,Ba and TiO_2:Rh,Sb have enough potential for water oxidation to form O_2. These energy levels were consistent with the H_2 and O_2 evolution abilities, as shown in Table 1. Of course, other kinetic factors of the active sites would exist for the H_2 and O_2 evolution abilities in addition to the energy levels of the thermodynamic factor.

Let us consider the reason why the Z-scheme systems shown in Table 2 are classified into three groups, based on the band structure and photoelectrochemical properties. Fig. 6 shows energy diagrams for the Z-schemes employing $Fe^{3+/2+}$ and $[Co(bpy)_3]^{3+/2+}$ redox couples at pH 2.4 and 4.0, respectively. It is assumed that the band levels shift with -0.059 V pH^{-1} because those materials are metal oxides.

$NaTaO_3$:Ir,La + $BiVO_4$ and $BaTa_2O_6$:Ir,La + $BiVO_4$ were active with a $[Co(bpy)_3]^{3+/2+}$ redox couple at pH 4.2, but not with $Fe^{3+/2+}$ at pH 2.4. Photogenerated holes in the Ir^{3+} levels in $NaTaO_3$:Ir,La and $BaTa_2O_6$:Ir,La (an H_2-evolving photocatalyst) possess small driving forces for oxidation of Fe^{2+} (an electron mediator) at pH 2.4 as shown in Fig. 6(a), whereas they possess enough potential for oxidation of $[Co(bpy)_3]^{2+}$ at pH 4.2 as shown in Fig. 6(b). The activities from the interparticle electron transfer were very small or negligible because of poor photoresponse and poor overlaps of the potentials giving cathodic photocurrents of $NaTaO_3$:Ir,La and $BaTa_2O_6$:Ir,La and an anodic photocurrent of $BiVO_4$ as shown in Fig. 5, and also may be due to poor contact between $NaTaO_3$:Ir,La or $BaTa_2O_6$:Ir,La (an H_2-evolving photocatalyst) and $BiVO_4$ (an O_2-

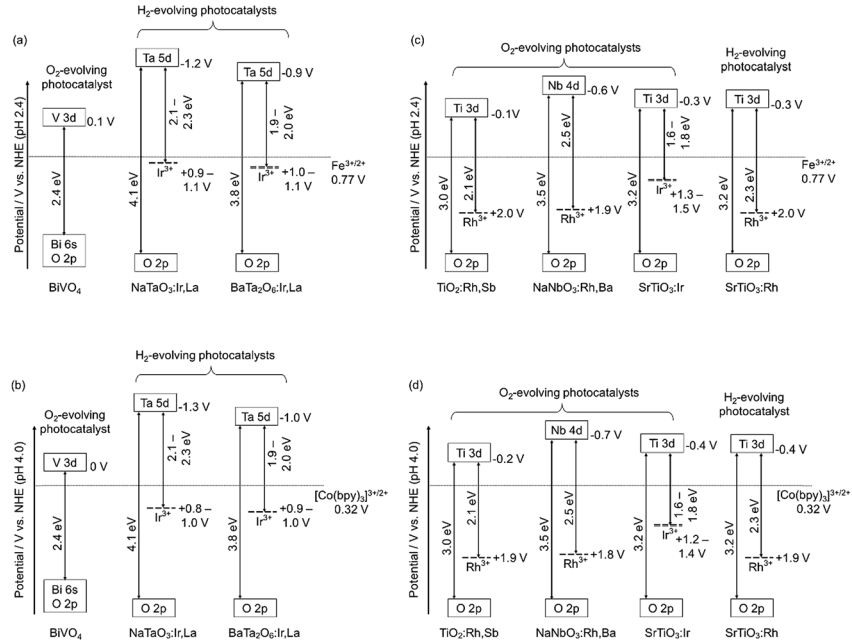

Fig. 6 The band structures of Rh- or Ir-doped metal oxide photocatalysts, and redox potentials of Fe and Co-complex ionic electron mediators at pH 2.4 and 4.0. (a) and (b) represent Z-scheme systems of Ir-doped metal oxides as H_2-evolving photocatalysts combined with $BiVO_4$. (c) and (d) represent Z-scheme systems of Rh-doped metal oxides and $SrTiO_3$:Ir as O_2-evolving photocatalysts combined with $SrTiO_3$:Rh.

evolving photocatalyst) in the suspension at pH 4.2. In contrast to them, $SrTiO_3$:Rh + $SrTiO_3$:Ir was active when the $[Co(bpy)_3]^{3+/2+}$ and $Fe^{3+/2+}$ redox couple ionic mediators were used, because the conduction band of $SrTiO_3$:Ir (an O_2-evolving photocatalyst) has enough potential for the reduction of Fe^{3+} and $[Co(bpy)_3]^{3+}$ (Fig. 6(c) and (d)). However, because the anodic photocurrent of $SrTiO_3$:Ir hardly overlapped with the cathodic photocurrent of $SrTiO_3$:Rh, the activities by interparticle electron transfer with and without RGO were negligible. The conduction bands of TiO_2:Rh,Sb and $NaNbO_3$:Rh,Ba (O_2-evolving photocatalysts) also possessed enough potential for the reduction of Fe^{3+} and $[Co(bpy)_3]^{3+}$ as well as $SrTiO_3$:Ir (Fig. 6(c) and (d)). Moreover, in these cases, the anodic photocurrents of the TiO_2:Rh,Sb and $NaNbO_3$:Rh,Ba photoelectrodes overlapped enough with the cathodic photocurrent of $SrTiO_3$:Rh. So, it is reasonable that $SrTiO_3$:Rh + $NaNbO_3$:Rh,Ba and $SrTiO_3$:Rh + TiO_2:Rh,Sb were active not only for the $[Co(bpy)_3]^{3+/2+}$ and $Fe^{3+/2+}$ redox couples but also *via* interparticle electron transfer with and without RGO. The activity of $SrTiO_3$:Rh + TiO_2:Rh,Sb was higher than that of $SrTiO_3$:Rh + $NaNbO_3$:Rh,Ba for all of the types of Z-scheme system. In the cases with the use of ionic electron mediators, it is probably due to the higher activity for O_2 evolution and the narrower energy gaps of TiO_2:Rh,Sb than those of $NaNbO_3$:Rh,Ba, as shown in Table 1. The reason why $SrTiO_3$:Rh + TiO_2:Rh,Sb showed a higher activity than $SrTiO_3$:Rh + $NaNbO_3$:Rh,Ba *via* interparticle electron transfer is that TiO_2:Rh,Sb gave much larger anodic photocurrents than $NaNbO_3$:Rh,Ba, as shown in Fig. 5.

Conclusions

We have successfully developed Z-scheme photocatalyst systems for water splitting under visible light irradiation employing Rh- and Ir-doped metal oxide photocatalysts with longer wavelength responses than conventional $SrTiO_3$:Rh and $BiVO_4$. The impurity levels of doped Ir^{3+} and Rh^{3+} that contributed to the visible light responses for the photocatalytic reactions were determined from diffuse reflectance spectra and supposing +3.0 V *vs.* NHE of a valence band of the oxide photocatalyst materials. The impurity levels of Ir^{3+} in $NaTaO_3$:Ir,La and $BaTa_2O_6$:Ir,La have sufficient potentials for the oxidation of the electron mediator $[Co(bpy)_3]^{2+}$, but insufficient potentials for water oxidation to form O_2 and oxidation of the electron mediator Fe^{2+}. The conduction bands of the $NaTaO_3$:Ir,La and $BaTa_2O_6$:Ir,La have enough potential for water reduction to form H_2. Therefore, the $NaTaO_3$:Ir,La and $BaTa_2O_6$:Ir,La could be used as H_2-evolving photocatalysts only when a $[Co(bpy)_3]^{3+/2+}$ redox couple was used. The impurity levels of Ir^{3+} in $SrTiO_3$:Ir and Rh^{3+} in TiO_2:Rh,Sb and $NaNbO_3$:Rh,Ba have potentials for water oxidation and their conduction bands possess the potentials for reduction of the electron mediators Fe^{3+} and $[Co(bpy)_3]^{3+}$. This property means that $SrTiO_3$:Ir, TiO_2:Rh,Sb and $NaNbO_3$:Rh,Ba could be employed as O_2-evolving photocatalysts for the construction of Z-scheme systems employing ionic electron mediators. Moreover, photoelectrochemical measurements using photocatalyst powders immobilized on conducting substrate revealed that the n-type characters and relatively negative onset potentials of the TiO_2:Rh,Sb and $NaNbO_3$:Rh,Ba photoanodes enabled the Z-scheme systems to work by interparticle electron transfer. Although the efficiencies of the present Z-scheme systems are low at the present stage, these will be improved by interfacial controls from a kinetic point of view in basic research. These results and discussion will contribute to the design of a highly active photocatalyst system for water splitting into H_2 and O_2, aiming for the demonstration of actual solar water splitting using a suitable reactor.

Conflicts of interest

There are no conflicts to declare.

Acknowledgements

This work was supported by JSPS KAKENHI Grant Numbers 17H06440 and 17H06433 in Scientific Research on Innovative Areas "Innovations for Light-Energy Conversion (I^4LEC)".

References

1 A. Kudo, H. Kato and I. Tsuji, *Chem. Lett.*, 2004, **33**, 1534.
2 A. Kudo and Y. Miseki, *Chem. Soc. Rev.*, 2009, **38**, 253.
3 F. E. Osterloh, *Chem. Mater.*, 2008, **20**, 35.
4 Y. Inoue, *Energy Environ. Sci.*, 2009, **2**, 364.
5 R. Abe, *J. Photochem. Photobiol., C*, 2010, **11**, 179.
6 T. Hisatomi, J. Kubota and K. Domen, *Chem. Soc. Rev.*, 2014, **43**, 7520.

7 K. Maeda and K. Domen, *Bull. Chem. Soc. Jpn.*, 2016, **89**, 627.
8 B. A. Pinaud, J. D. Benck, L. C. Seitz, A. J. Forman, Z. Chen, T. G. Deutsch, B. D. James, K. N. Baum, G. N. Baum, S. Ardo, H. Wang, E. Miller and T. F. Jaramillo, *Energy Environ. Sci.*, 2013, **6**, 1983.
9 D. M. Fabian, S. Hu, N. Singh, F. A. Houle, T. Hisatomi, K. Domen, F. E. Osterloh and S. Ardo, *Energy Environ. Sci.*, 2015, **8**, 2825.
10 T. Yamada and K. Domen, *Chem. Eng.*, 2018, **2**, 36.
11 A. Kudo, in *"Photocatalysis", Contemporary Catalysis; Science, Technology and Applications*, ed. P. Kamer, D. Vogt and J. Thybaut, Royal Society of Chemistry, Cambridge, 2017, ch. 3.7, pp. 326–343.
12 A. J. Bard, *J. Photochem.*, 1979, **10**, 59.
13 A. Kudo, *MRS Bull.*, 2011, **36**, 32.
14 K. Maeda, *ACS Catal.*, 2013, **3**, 1486.
15 Y. Wang, H. Suzuki, J. Xie, O. Tomita, D. J. Martin, M. Higashi, D. Kong, R. Abe and J. Tang, *Chem. Rev.*, 2018, **118**, 5201.
16 H. Kato, M. Hori, R. Konta, Y. Shimodaira and A. Kudo, *Chem. Lett.*, 2004, **33**, 1348.
17 Q. Wang, T. Hisatomi, Q. Jia, H. Tokudome, M. Zhong, C. Wang, Z. Pan, T. Takata, M. Nakabayashi, N. Shibata, Y. Li, I. D. Sharp, A. Kudo, T. Yamada and K. Domen, *Nat. Mater.*, 2016, **15**, 611.
18 Q. Wang, T. Hisatomi, Y. Suzuki, Z. Pan, J. Seo, M. Katayama, T. Minegishi, H. Nishiyama, T. Takata, K. Seki, A. Kudo, T. Yamada and K. Domen, *J. Am. Chem. Soc.*, 2017, **139**, 1675.
19 Q. Wang, T. Hisatomi, M. Katayama, T. Takata, T. Minegishi, A. Kudo, T. Yamada and K. Domen, *Faraday Discuss.*, 2017, **197**, 491.
20 R. Konta, T. Ishii, H. Kato and A. Kudo, *J. Phys. Chem. B*, 2004, **108**, 8992.
21 R. Niishiro, S. Tanaka and A. Kudo, *Appl. Catal., B*, 2014, **150**, 187.
22 S. Suzuki, H. Matsumoto, A. Iwase and A. Kudo, *Chem. Commun.*, 2018, **54**, 10606.
23 A. Iwase and A. Kudo, *Chem. Commun.*, 2017, **53**, 6156.
24 A. Iwase, K. Saito and A. Kudo, *Bull. Chem. Soc. Jpn.*, 2009, **82**, 514.
25 R. Niishiro, R. Konta, H. Kato, W. J. Chun, K. Asakura and A. Kudo, *J. Phys. Chem. C*, 2007, **111**, 17420.
26 A. Kudo, K. Omori and H. Kato, *J. Am. Chem. Soc.*, 1999, **121**, 11459.
27 A. Iwase, H. Kato and A. Kudo, *J. Sol. Energy Eng.*, 2010, **132**, 21106.
28 Y. Sasaki, A. Iwase, H. Kato and A. Kudo, *J. Catal.*, 2008, **259**, 133.
29 Y. Sasaki, H. Kato and A. Kudo, *J. Am. Chem. Soc.*, 2013, **135**, 5441.
30 A. Iwase, Y. H. Ng, Y. Ishiguro, A. Kudo and R. Amal, *J. Am. Chem. Soc.*, 2011, **133**, 11054.
31 K. Iwashina, A. Iwase, Y. H. Ng, R. Amal and A. Kudo, *J. Am. Chem. Soc.*, 2015, **137**, 604.
32 A. Iwase, S. Yoshino, T. Takayama, Y. H. Ng, R. Amal and A. Kudo, *J. Am. Chem. Soc.*, 2016, **138**, 10260.
33 Y. Sasaki, H. Nemoto, K. Saito and A. Kudo, *J. Phys. Chem. C*, 2009, **113**, 17536.
34 Q. Jia, A. Iwase and A. Kudo, *Chem. Sci.*, 2014, **5**, 1513.
35 W. S. Hummers and R. E. Offeman, *J. Am. Chem. Soc.*, 1958, **80**, 1339.
36 K. Iwashina and A. Kudo, *J. Am. Chem. Soc.*, 2011, **133**, 13272.
37 S. Kawasaki, K. Akagi, K. Nakatsuji, S. Yamamoto, I. Matsuda, Y. Harada, J. Yoshinobu, F. Komori, R. Takahashi, M. Lippmaa, C. Sakai, H. Niwa, M. Oshima, K. Iwashina and A. Kudo, *J. Phys. Chem. C*, 2012, **116**, 24445.

38 S. Kawasaki, R. Takahashi, K. Akagi, J. Yoshinobu, F. Komori, K. Horiba, H. Kumigashira, K. Iwashina, A. Kudo and M. Lippmaa, *J. Phys. Chem. C*, 2014, **118**, 20222.
39 D. E. Scaife, *Sol. Energy*, 1980, **25**, 41.
40 S. Kawasaki, K. Nakatsuji, J. Yoshinobu, F. Komori, R. Takahashi, M. Lippmaa, K. Mase and A. Kudo, *Appl. Phys. Lett.*, 2012, **101**, 033910.
41 K. Sayama, A. Nomura, Z. Zou, R. Abe, Y. Abe and H. Arakawa, *Chem. Commun.*, 2003, 2908.
42 K. Sayama, A. Nomura, T. Arai, T. Sugita, R. Abe, M. Yanagida, T. Oi, Y. Iwasaki, Y. Abe and H. Sugihara, *J. Phys. Chem. B*, 2006, **110**, 2908; F. F. Adbi, L. Han, A. H. M. Smets, M. Zeman, B. Dam and R. van de Krol, *Nat. Commun.*, 2013, **4**, 2195.
43 Y. Park, K. J. McDonald and K.-S. Choi, *Chem. Soc. Rev.*, 2013, **42**, 2321.
44 Q. Jia, K. Iwashina and A. Kudo, *Proc. Natl. Acad. Sci. U. S. A.*, 2012, **109**, 11564.
45 M. Yamaguchi, R. Niishiro, Q. Jia, Y. Kuang, K. Kitamura, A. Iwase, T. Minegishi, T. Yamada, K. Domen and A. Kudo, to be submitted.